J. Geogr. Sci. 2023, 33(3): 449-463
DOI: https://doi.org/10.1007/s11442-023-2091-0

An overall consistent increase of global aridity in 1970–2018

LUO Dengnan[1], *HU Zhongmin[2,3], DAI Licong[2], HOU Guolong[1], DI Kai[1], LIANG Minqi[1], CAO Ruochen[4], ZENG Xiang[1]

1. School of Geography, South China Normal University, Guangzhou 510631, China;
2. Key Laboratory of Agro-Forestry Environmental Processes and Ecological Regulation of Hainan Province, Hainan University, Haikou 570228, China;
3. Southern Marine Science and Engineering Guangdong Laboratory (Zhuhai), Zhuhai 519082, Guangdong, China;
4. International Institute for Earth System Sciences, Nanjing University, Nanjing 210023, China

Abstract: Climate change is expected to introduce more water demand in the face of diminishing water supplies, intensifying the degree of aridity observed in terrestrial ecosystems in the 21st century. This study investigated spatiotemporal variability within global aridity index (AI) values from 1970–2018. The results revealed an overall drying trend (0.0016 yr^{-1}, p<0.01), with humid and semi-humid regions experiencing more significant drying than other regions, including those classified as arid or semi-arid. In addition, the Qinghai-Tibet Plateau has gotten wetter, largely due to the increases in precipitation (PPT) observed in that region. Global drying is driven primarily by decreasing and increasing PPT and potential evapotranspiration (PET), respectively. Decreases in PPT alone or increases in PET also drive global aridification, though to a lesser extent. PPT and increasing potential evapotranspiration (PET), with increasing PET alone or decreasing PPT alone. Slightly less than half of the world's land area has exhibited a wetting trend, largely owing to increases in regional PPT. In some parts of the world, the combined effects of increased PPT and decreased PET drives wetting, with decreases in PET alone explaining wetting in others. These results indicate that, without consideration of other factors (e.g., CO_2 fertilization), aridity may continue to intensify, especially in humid regions.

Keywords: aridity index; climate change; arid area; drying trend

1 Introduction

Increasing aridity, a manifestation of climate change, is a serious threat to ecosystems (Huang *et al*., 2016b; Zhao *et al*., 2020; Hu *et al*., 2022). Declining rainfall has resulted in

Received: 2022-02-21 **Accepted:** 2022-09-06
Foundation: National Natural Science Foundation of China, No.31922053; The Second Tibetan Plateau Scientific Expedition and Research Program, No.2019QZKK0405; The Hainan University Start-up Fund, No.KYQD(ZR)21096; The Key R&D Program of Hainan, No.ZDYF2022SHFZ042
Author: Luo Dengnan (1997–), MS, specialized in extreme events and terrestrial ecosystem carbon cycle. E-mail: 2020022625@m.scnu.edu.cn.
*Corresponding author: Hu Zhongmin, Professor, E-mail: huzm@hainanu.edu.cn

the expansion of the area classified as arid or semi-arid (Dai, 2012; Sheffield *et al*., 2012; Huang *et al*., 2016a), and the frequency and intensity of droughts are projected to increase as global change continues (Strzepek *et al*., 2010; Asadi Zarch *et al*., 2015). This expansion of aridity is the result of an imbalance between water supply and demand. Empirically based models predict that the intensity and duration of drought will increase due to the increase in potential evaporation rate driven by rising temperatures and regional decreases in precipitation (Dai, 2012). This will make the impacted terrestrial ecosystems more vulnerable and sensitive to climate change (Lian *et al*., 2021; Zeng *et al*., 2022). In order to understand how terrestrial ecosystems may change in response to climate change, it is crucial to assess variability in dryness across the biosphere and the factors driving it.

An aridity index (AI) is a widely used metric that quantifies aridity. Scientists have developed various AIs based on meteorological factors such as temperature, precipitation, and potential evapotranspiration (PET) (Necula *et al*., 1998; Arora, 2002; Li *et al*., 2019). The AI proposed by the Food and Agriculture Organization (FAO) of the United Nations is defined as the ratio of precipitation to PET (Allen *et al*., 1998). It is clear, simple, and practical to use and is effectively used in assessments of aridity (Greve *et al*., 2019; Zhou *et al*., 2020).

Many studies have used the FAO AI to assess aridity in different regions. For example, Huang *et al*. (2016b) found that the expansion of drylands occurs mainly in semi-arid regions around the world due to decreasing values of AI in these regions. Mu *et al*. (2013) found that the Asia-Pacific region experienced more frequent and intense drought events from 2000 to 2011. Dryness in Iraq increased significantly from 1980 to 2011, with drought severity increasing since 1997 owing to a reduction in precipitation and an increase in temperature (Şarlak and Mahmood Agha, 2018). Although a few studies have reported interannual variability in the aridity of humid regions (Ullah *et al*., 2022), most have focused either on drylands (Mu *et al*., 2013; Asadi Zarch *et al*., 2015; Huang *et al*., 2016a; Pan *et al*., 2021) or on regions in close proximity to the studies' authors (Huo *et al*., 2013; Zhao *et al*., 2017; Li *et al*., 2019; Tsiros *et al*., 2020). Additionally, most previous studies have focused on the temporal dynamics of AI values at an annual scale based on global mean AI (Dai, 2012; Ullah *et al*., 2022). However, AI values change seasonally, and how these changes vary across different continents and climate regions is poorly understood. For example, Dai (2012) and Ullah (2022) investigated temporal trends in aridity at the global scale, but whether supply (precipitation) or demand (PET) drives AI dynamics remains unclear. An understanding of the factors driving these changes is important for predicting future changes in AI. Therefore, it is urgent to have a better developed understanding of the spatiotemporal dynamics of and dominant factors driving aridity in humid regions.

Here we use data for precipitation (PPT) and PET from the Climatic Research Unit (CRU) v4.03 product dataset to calculate FAO AI to clarify the spatial-temporal variabilities in climate dryness at the global scale. We selected 1970 as the starting year because it approximates the beginning of two trends: an acceleration in global warming and increasingly frequent global drought (Visbeck *et al*., 2001; Dai, 2012). This study aims to answer the following questions: 1) How has global climate aridity changed on seasonal and annual scales over the past five decades (1970–2018) and how has it varied across climate regions and continents? 2) What are the dominant factors controlling variability in AI?

2 Data and methods

2.1 Data

The PPT and PET data used in this study were produced by CRU (http://www.cru.uea.ac.uk/cru/data/hrg) at the University of East Anglia in the United Kingdom. The CRU dataset was aggregated from records with a spatial resolution of 0.5°×0.5° that were collected monthly from 1901–2018. The accuracy of the CRU dataset has been confirmed independently (Van Der Schrier *et al*., 2013; Harris *et al*., 2020). PET data is calculated by the Penman-Monteith equation suggested by the FAO (Harris *et al*., 2020). As described above, FAO AI is defined as the ratio of annual precipitation to annual potential evapotranspiration:

$$AI = PPT / PET \tag{1}$$

where *PPT* and *PET* are the annual precipitation (mm) and the annual potential evapotranspiration (mm), respectively. The larger the value of *AI*, the wetter the climate. Dryness can be divided into 5 levels by AI value: humid (AI$\geqslant$0.65), semi-humid (0.5$\leqslant$AI<0.65), semi-arid (0.2$\leqslant$AI<0.5), arid (0.05$\leqslant$AI<0.2), and extreme arid (AI<0.05) (Huang *et al*., 2016a; Zhou *et al*., 2018).

2.2 Data analysis

The CRU TS v4.03 dataset was used to calculate values of AI from 1970 to 2018. A linear regression model was used to calculate the trend values of AI, PPT and PET. The Thiel-Sen's trend analysis and Mann-Kendall tests were applied to assess significance of trends in AI over 1970–2018. Finally, the contribution of meteorological factors to AI variabilities was quantified for each pixel. The effect of latitude on pixel area was taken into account when calculating global average values by projecting the raster data with EASE-Grid 2.0 Global (https://nsidc.org/data/user-resources/help-center/guide-ease-grids).

Linear regression

Regression statistics were used to calculate the trend for the annual average time series of AI globally and for each continent except Antarctica. Eq. (3) shows the univariate linear regression model of AI:

$$Y_i = at_i + b \tag{2}$$

where Y_i represents the variable (AI, PPT and PET) for a given year$_i$, a represents the linear trend of the variable, t_i is the year, and b is the intercept. Positive values of a indicate that the variable increases over time; negative values indicate decreasing values.

Sen's slope and Mann-Kendall test

Theil-Sen median trend analysis is a robust non-parametric statistical calculation method. Sen's slope is calculated as follows:

$$\beta = Median\left(\frac{x_j - x_i}{j - i}\right), \forall j > i \tag{3}$$

where β represents Sen's trend, x_i and x_j represent the value of the time series at time i and time j, respectively, 1970$\leqslant i \leqslant j \leqslant$2018. A positive value of β indicates an upward trend in the time series; A β value of 0 indicates no obvious trend; A negative value of β indicates a downward trend in the time series. Trend estimation was improved by calculating the medi-

an slope of the combination of $n(n–1)/2$.

The Mann-Kendall test is a non-parametric statistical test recommended by the World Meteorological Organization and is widely applied in the assessment of aridity (Ahmed *et al*., 2019; Cao and Zhou, 2019), precipitation (Ahmed *et al*., 2019), potential evapotranspiration (Cao and Zhou, 2019), etc. The Mann-Kendall trend test statistic S is calculated as follows:

$$S = \sum_{i=1}^{n-1} \sum_{j=i+1}^{n} sign(x_j - x_i) \tag{4}$$

$$sign(\varepsilon) = \begin{cases} -1, & \varepsilon < 0 \\ 0, & \varepsilon = 0 \\ 1, & \varepsilon > 0 \end{cases} \tag{5}$$

where x represents AI, PPT or PET.

Mann and Kendall demonstrated that when $n \geqslant 8$, E(S)=0, variance can be calculated by:

$$Var(S) = \frac{n(n-1)(2n+5) - \sum_{k=1}^{m} t_k (t_k - 1)(2t_k + 5)}{18} \tag{6}$$

where n is the number of values in the time series, m is the number of repeated data groups in the sequence, and t_k is the number of repeated values in the k-th repeated data group.

When $n \geqslant 10$, the statistic S is approximately normally distributed. To test significance, we used the test statistic Z, which is calculated as follows:

$$Z = \begin{cases} \dfrac{S+1}{\sqrt{Var(S)}}, & S > 0 \\ 0, & S = 0 \\ \dfrac{S-1}{\sqrt{Var(S)}}, & S < 0 \end{cases} \tag{7}$$

In this study, the length of the time series is 49 years, so Z is used for bilateral trend testing. At a given significance level α, we identify the critical value $Z_{1-\alpha/2}$ in the normal distribution table. When $\beta>0$ and $|Z| \leqslant Z_{1-\alpha/2}$, the time series is increasing but the trend is non-significant; when $\beta>0$ and $|Z|>Z_{1-\alpha/2}$, the time series is increasing and the trend is significant; when $\beta=0$, no significant trend exists in time series; when $\beta<0$ and $|Z| \leqslant Z_{1-\alpha/2}$, the time series declines but the trend is non-significant; when $\beta<0$ and $|Z|>Z_{1-\alpha/2}$, the time series shows a significantly decreasing trend.

3 Results

3.1 Temporal trends and spatial patterns of AI from 1970–2018

Globally, dry areas (AI<0.5) are primarily distributed across middle and low latitudes, including North Africa, southwest North America, central Asia, and Australia. Major hyper arid areas (AI<0.05) are typically located in areas classified as deserts, such as the Taklimakan Desert, the Sahara Desert, and the Rub al Khali Desert (Figure 1a). The total area of drylands with AI<0.65 is 44.87×10^6 km^2. Hyper arid regions occupy an area of 8.20×10^6 km^2 (Figure 1b).

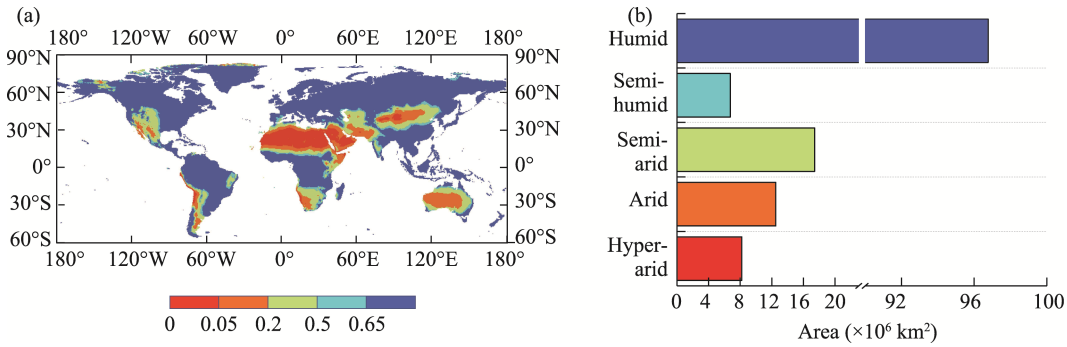

Figure 1 Multi-year mean of AI from 1970–2018 (a. Global distribution of AI; b. Total land cover associated with different aridity regimes)

AI shows an overall decreasing trend from 1970–2018 (0.0016 yr^{-1}, p<0.01), suggesting that the climate has been getting drier over the past five decades (Figure 2a). Annual precipitation exhibits a slight increasing trend with high inter-annual variability (p=0.15). In contrast, PET shows a significant increasing trend (p<0.01) with a rate of increase of 0.0592 mm yr^{-1}, almost three times faster than rate of PPT increase (0.017 mm yr^{-1}) (Figures 2b and

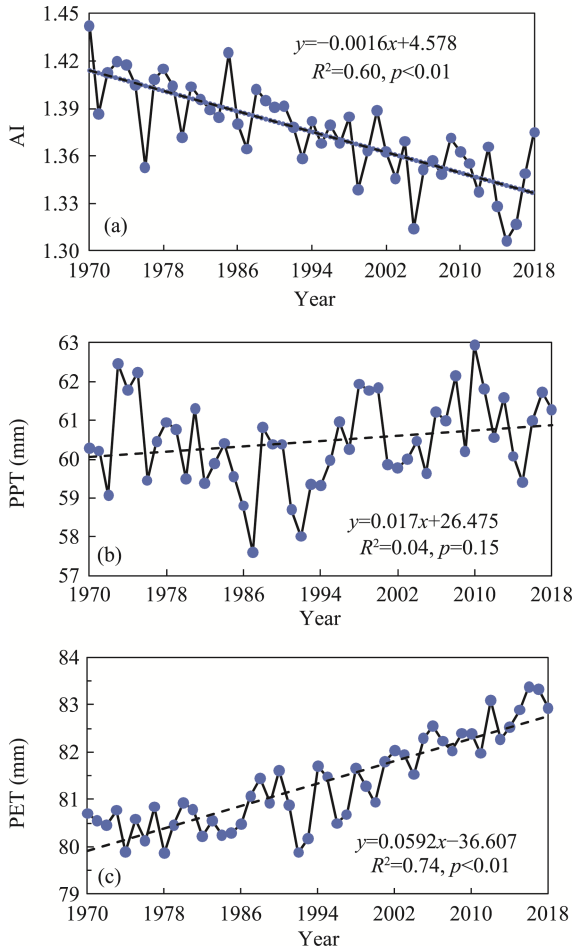

Figure 2 Trends in global averages for AI (a), PPT (b), and PET (c) from 1970–2018 (R^2 is the coefficient of determination)

2c). These results suggest that decreasing values of AI are mostly due to increasing water demand (i.e., PET).

AI decrease significantly over 1970–2018 (p<0.05) for all continents except Europe (Figure 3). AI values associated with Oceania and South America show the largest rates of change, both decreasing at 0.015 per decade, suggesting a severe increase in aridity across these two continents (Figures 3a–3f). Increasing aridity in these regions was associated with increasing PET (p<0.01) and decreasing PPT (Figures 3k and 3l). Although PPT increased in Africa and Asia, these increases were overwhelmingly offset by strongly increasing PET, resulting in the increasing aridity observed in these regions (Figures 3g, 3h, 3m and 3n).

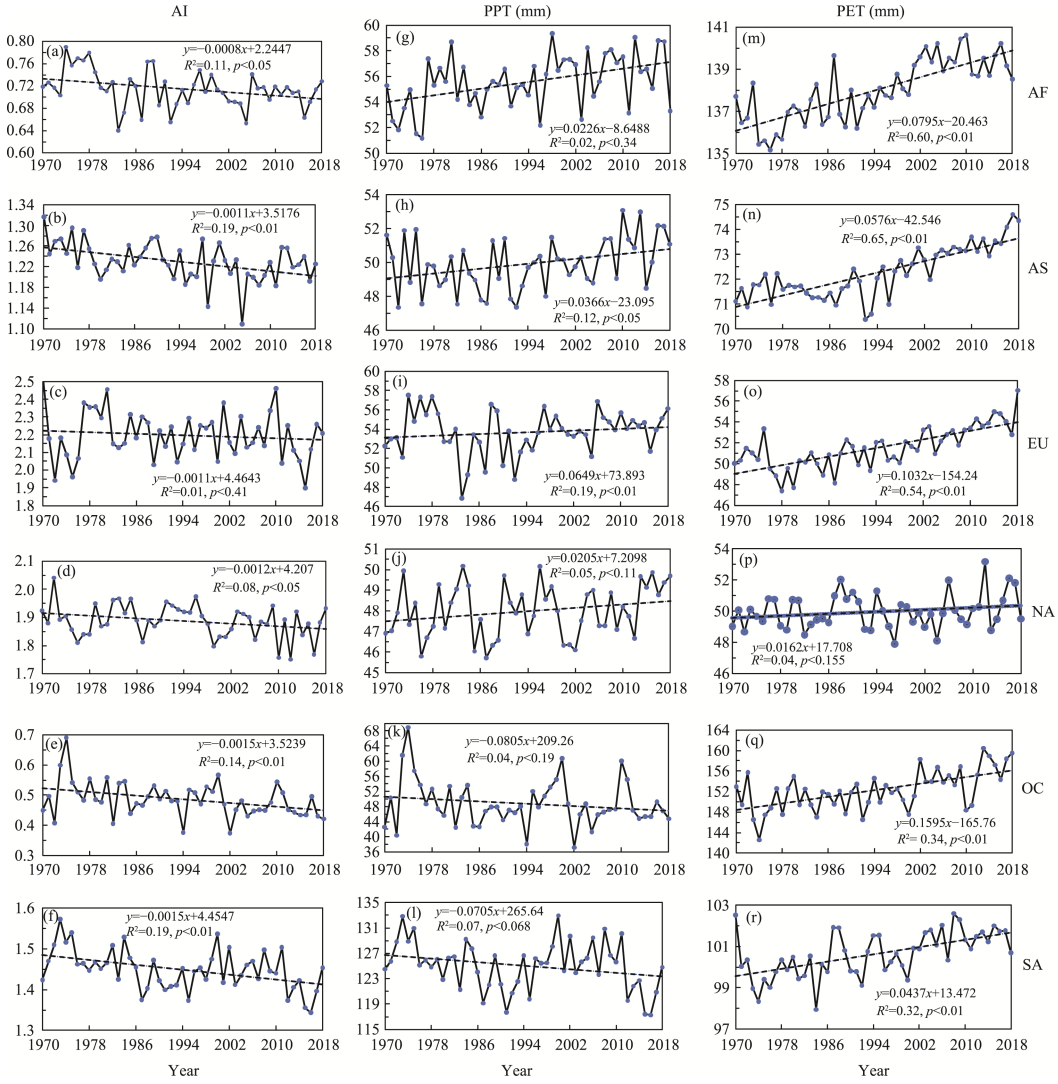

Figure 3 Inter-annual variability and temporal trends in AI, PPT, and PET across different continents (AF: Africa; AS: Asia; EU: Europe; NA: North America; OC: Oceania; SA: South America)

Trends observed in AI values show high spatial heterogeneity. For example, AI has decreased over the last five decades in Australia, Eastern Asia, Northern Africa, Southern Africa, Southern America, southwestern North America, around the Mediterranean, and north-

ern Greenland, accounting for 52.53% (10.9% at $p<0.05$ and 15.23% at $p<0.1$) of global land area (Figure 4a). Previous studies have confirmed that aridity has been worsening in Northern Africa (Lickley and Solomon, 2018). Although precipitation over 60.09% of the global area (17.99% at $p<0.1$) increased over the period investigated (Figure 4b), the positive contribution to climate wetness is overwhelmingly offset by the increase in PET. Globally, PET has increased in all regions except Southeast Asia, western South America, and central and northern North America, and accounts for 81.74% of global land area ($p<0.05$) (Figure 4c). These results suggest that the decreasing AI is mainly driven by the increasing water demand (i.e., PET).

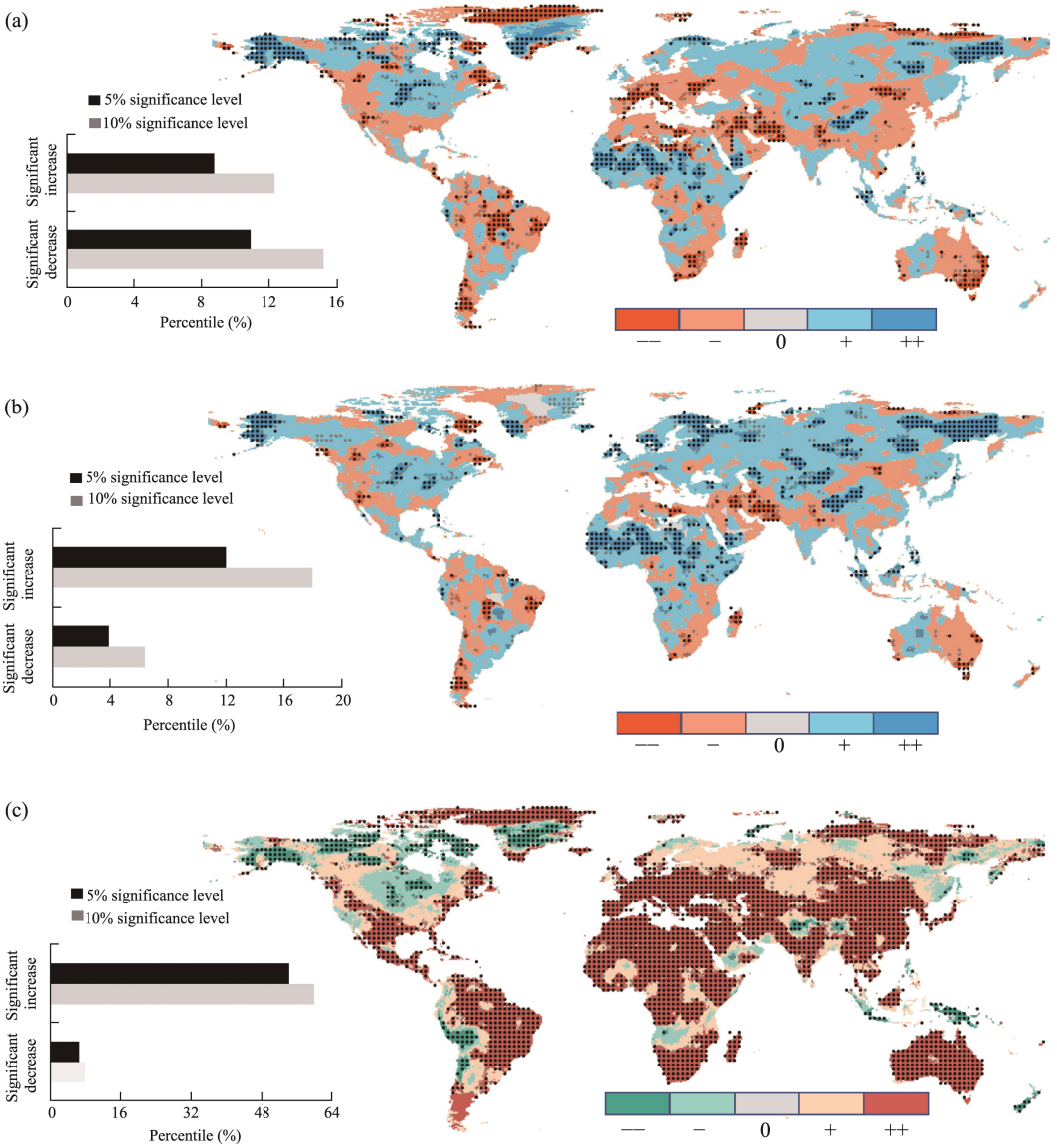

Figure 4 Spatial variability and trends in AI (a), PPT (b), and PET (c) across the globe. — and – denote a significant ($p<0.05$) and non-significant ($p>0.05$) decline, respectively. '0' indicates no obvious trend and + and ++ denote a non-significant and significant increase, respectively. The black and gray bars denote significance at the 95% and 90% confidence levels, respectively. Black points indicate significance at the 95% confidence level.

Overall, AI exhibited an overall decrease across all seasons except for spring in Asia and spring and summer in South America, suggesting that increasing dryness is a global trend (Figure 5a). Although PPT increased in all regions except Oceania, South America, and Africa in the spring (Figure 5b), this is overwhelmingly offset by the increase observed in PET (Figure 5c), leading to an overall AI decrease in Africa, Asia, Europe and North America. Furthermore, the combination of decreased PPT and increased PET has resulted in greater dryness in Oceania and South America.

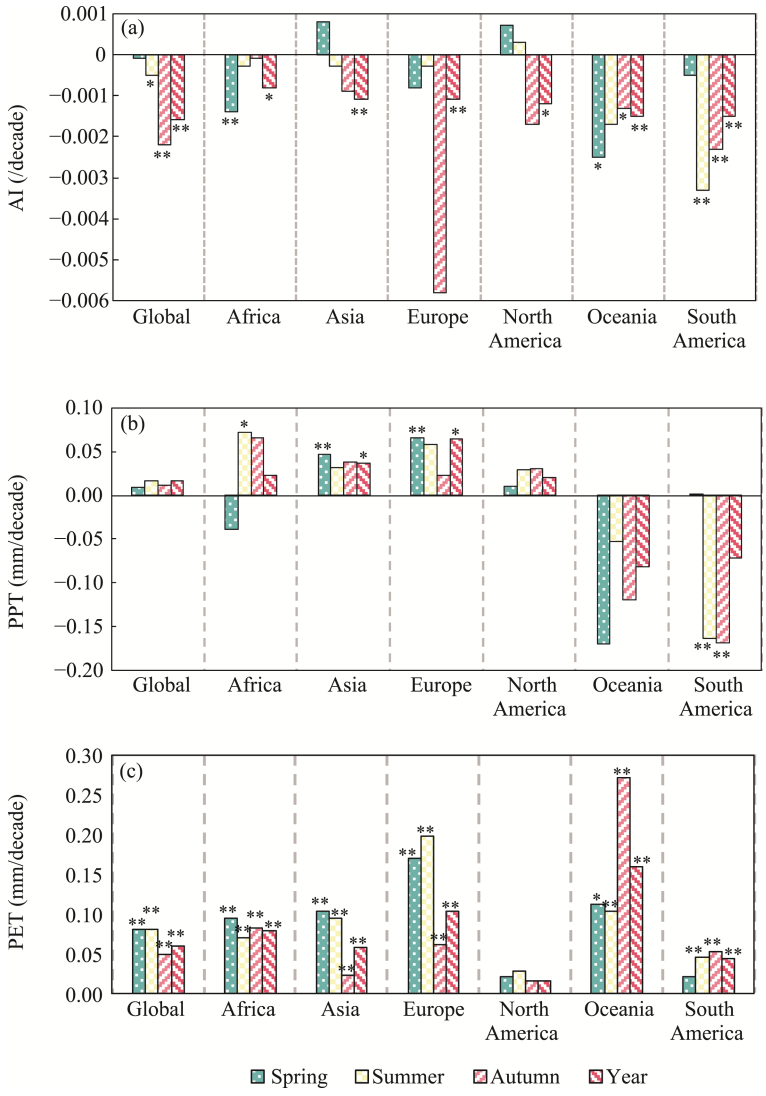

Figure 5 Trends in AI, PPT, and PET in different seasons (Spring: March to May; Summer: June to August; Autumn: September to November). Far northern areas are covered with ice in the winter, so this season is ignored. * and ** represent the significance at the 95% and 99% confidence level, respectively.

We found that both annual and seasonal values of AI exhibited overall decreases in humid and semi-humid regions except in humid regions at springtime (Figure 6a). Surprisingly, AI in the humid regions displayed the most obvious decreasing trend (0.025 per decade), fol-

lowed by the semi-humid and semi-arid regions. However, AI in arid regions showed slight increases in autumn and over the whole year, suggesting the emergence of a wetting trend. In comparison, PPT displays greater variability across different climate regions. Annual PPT in humid, semi-humid, and semi-arid regions shows overall increases, but PPT decreases in humid regions during the autumn. The largest decreases in AI were observed in hyper-arid regions at springtime (Figure 6b). PET increased both annually and seasonally, with increases in spring and summer greater than those in the autumn or the whole year (Figure 6c).

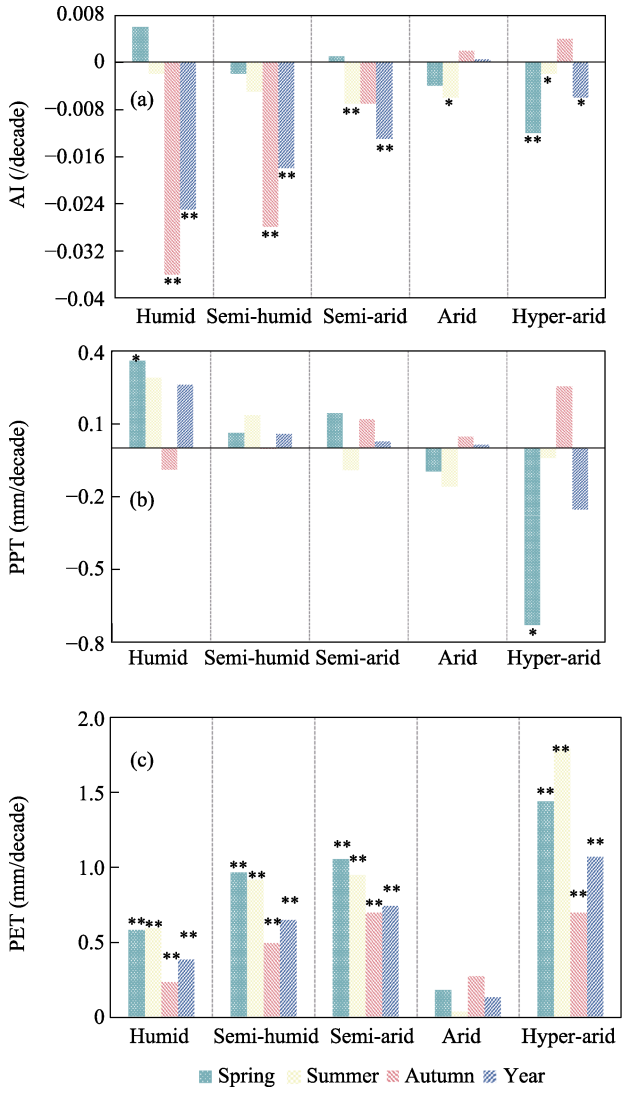

Figure 6 Seasonal trends in AI, PPT and PET across different climate regions, demonstrating the same pattern as those illustrated in Figure 5

3.2 Factors driving temporal trends in AI

Increasing aridity is observed at the global scale, with 52.53% of land area exhibiting a drying trend. This pattern is mainly driven by decreasing PPT and increasing PET (accounting

for 30.91%), with some of the pattern resulting from increases in PET alone (accounting for 18.51%) or decreases in PPT alone (accounting for 3.11%). In comparison, areas experiencing wetting trends account for 47.35% of land area globally. Wetting is the result of increasing PPT (accounting for 32.43%), the combined effects of increasing PPT and decreasing PET (accounting for 10.82%), and decreasing PET (accounting for 4.10%) (Figure 7). Dryness in tropical rainforests is mainly caused by the combined effects of the decreasing PPT and increasing PET, whereas the humidification of the Qinghai-Tibet Plateau is mainly induced by increasing PPT.

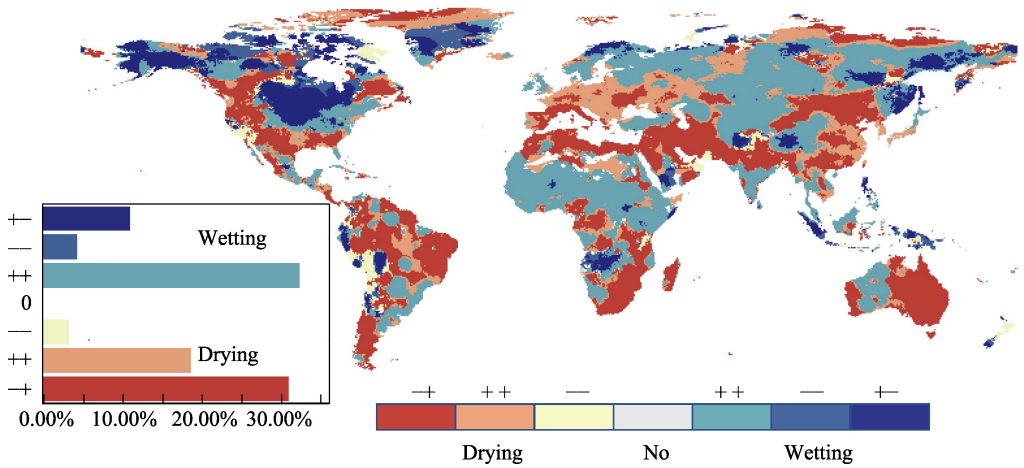

Figure 7 Spatial distribution of dry and wet conditions at the global scale. In areas experiencing increased aridity, –+ denotes that dryness results from the combined effects of PPT and PET, ++ and — denote that the dryness is derived from increased PET or decreased PPT, respectively. "No" denotes no significant drying or wetting trend. In areas experiencing wetting, +– denotes that wetting results from the combined effects of PPT and PET, ++ and — denote that wetness results from increased PPT or decreased PET, respectively. The histogram on the left shows the proportions of drying and wetting.

4 Discussion

4.1 Trends in global AI over 1970–2018

We found that AI has decreased at the global scale from 1970–2018, owing to increasing PET (Figure 5), which has ultimately resulted in an overall increase in global aridity. This finding is consistent with previous studies, in which increasing aridity is reported in arid regions (Dai, 2012; Huang *et al*., 2016a, 2016b). Although decreasing values of AI are observed in most areas, some places, such as East Africa, Russia, Southeast Asia, north of North America, and Qinghai-Tibet Plateau, exhibit increases. Increasing global temperatures are accelerating increases observed in PET, which results in accelerating aridification. However, increases in PET do not necessarily mean that vegetation will experience higher degrees of water stress. Some studies have found that values of vegetation indices such as the Normalized Difference Vegetation Index (NDVI) have increased in drylands since the 1980s (Fensholt *et al*., 2012; Donohue *et al*., 2013; Swann *et al*., 2016). These increases in NDVI may be attributed to higher water use efficiency induced by increased atmospheric CO_2, potentially alleviating the negative effects of increasing aridity on vegetation (Yang *et*

al., 2016). It should be noted that increasing global temperatures will also increase vapor pressure deficit (VPD) (Ficklin and Novick, 2017), potentially further increasing PET and exacerbating aridity in the future (Swann *et al*., 2016).

We observed a trend of severe autumn drought in Europe, which is consistent with the findings by Spinoni *et al*. (2017). This seasonal drought may be due to the influence of natural variability such as ENSO (Muñoz-Díaz and Rodrigo, 2005; Pieper *et al*., 2020). Moreover, we find that the trend of decreasing AI observed in humid and semi-humid regions, especially in tropical rainforest areas, is more obvious than that observed in arid or semi-arid areas. Similarly, projections by De Oliveira *et al*. (2018) indicated that the Amazon Basin will get drier, and precipitation in the Amazon is predicted to decrease with global warming (Li *et al*., 2021). Most previous studies have focused mainly on arid and semi-arid areas (Dai, 2012; Cook *et al*., 2014; Huang *et al*., 2016b), with little consideration given to humid and semi-humid regions (Ullah *et al*., 2022). In light of our findings, it is important to pay more attention to humid and semi-humid regions in the future, especially in the context of intensifying aridity. The drying trend in humid and semi-humid regions can be attributed to the faster increases observed in PET relative to those observed in PPT, which attenuates the effect of increased PPT on AI. Moreover, land-atmosphere interactions and human activity are additional factors promoting this trend. These results suggest that the conversion of humid and semi-humid climates to arid or semi-arid climates may be an additional consequence of climate change. (Huang *et al*., 2019). In addition, it is worth mentioning that the wetting trend observed in the Qinghai-Tibet Plateau may be ascribed to increasing PPT (Figure 4) resulting from greening vegetation and the Indian monsoon in the region (Wu *et al*., 2007; Li *et al*., 2020).

4.2 Factors driving trends in AI from 1970–2018

Our findings illustrate that global drying trends are mainly the result of increasing PET. Although PPT in Africa and Asia exhibited slight increases, enhanced rainfall is overwhelmingly offset by large increases in PET, ultimately resulting in increased aridity across these continents. Importantly, decreasing PPT and increasing PET in central and eastern Australia may result in intensifying drying and more frequent wildfires in these regions (Nohan *et al*., 2016; Brando *et al*., 2019).

Climate change not only intensifies the hydrological cycle, but also increases interannual variability, regional and seasonal differences in precipitation, (Zhou *et al*., 2021) and the frequency of extreme precipitation events across the globe (IPCC, 2021). Climate change also has a profound impact on atmospheric circulation, weakening the West African and East Asian monsoons (Huang *et al*., 2016a) to decrease PPT in northern African and southeastern China. This results in drier conditions in these areas (Figures 4a and 4b). In addition, abnormal sea surface temperatures (SST) have strengthened local circulation (Chang *et al*., 2000). For instance, the frequency of positive IOD (Indian Ocean Dipole) values has increased significantly in the past 50 years, resulting in a wetter East Africa and a drier southern Australia (Saji *et al*., 1999; Saji and Yamagata, 2003). However, the Qinghai-Tibet Plateau and eastern China have experienced slightly increased wetting, especially in the autumn months (Li *et al*., 2020). Wetting in the Qinghai-Tibet Plateau is mainly ascribed to increasing PPT (Li *et al*., 2010; Feng *et al*., 2020). Drying observed in the Amazon tropical rain-

forest is caused primarily by the combined effects of decreased PPT and increased PET. In terms of AI, the importance of PPT has decreased as changes to PET have intensified (Dai, 2012; Huang *et al*., 2017; Pan *et al*., 2021), especially in Oceania and South America (Figures 5 and 7). In general, increasing global temperatures greatly increase PET and reduce precipitation, further intensifying aridification (Van Der Schrier *et al*., 2013).

We find that the trend toward dryness observed in humid and semi-humid regions is more obvious than that observed in arid or semi-arid areas. In contrast, many arid areas, including southern India, the east coast of Africa, and central and western Australia, are getting wetter (Figure 4). Increases in wetness are due to increasing PPT. Previous studies have found that changes in SST in the Indian Ocean promote changes in regional atmospheric circulation, increasing the potential for further increases in PPT in these areas (Saji *et al*., 1999; Saji and Yamagata, 2003; Cherchi and Navarra, 2013). Furthermore, enhancement of the southwest summer monsoon (Huang *et al*., 2016a) and the continuing intensification of human activity (Hoerling *et al*., 2010) could promote additional increases in PPT in southern India.

Our findings have important implications for understanding aridity and ecosystem response to aridity under continuous and substantial warming. The trend of increasing dryness observed in humid and semi-humid regions (e.g., tropical rainforests) is of particular concern. Furthermore, persistent increases in aridity will likely result in more frequent wildfires and heat waves (Brando *et al*., 2019; Bastos *et al*., 2020), which could impose additional stress on humid and semi-humid ecosystems. Further research is needed to investigate the effects of other factors (e.g., CO_2, solar radiation, etc.) on spatiotemporal patterns of aridification.

5 Conclusions

Our results show an overall decrease in values of the global aridity index from 1970–2018 owing to increasing water demand (i.e., PET), suggesting that the global climate has gotten drier over the past five decades. Annually, aridity has increasing rapidly across all continents, and humid and semi-humid regions have experienced disproportionate increases in dryness. Seasonally, all continents have exhibited increasing aridity in autumn, with humid and semi-humid regions experiencing particularly high rates of autumnal aridification. Furthermore, diverging from historical patterns, the decreases in AI values observed in humid and semi-humid regions are greater than those in arid or semi-arid regions. At the same time, hyper-arid regions continue to get drier. Overall, the drying trend observed is primarily caused by increasing PET. We expect aridification to continue to intensify concomitant with increasing global PET, especially in humid and semi-humid regions

Data availability statement

The precipitation and potential evapotranspiration were downloaded from the Climate Change Research Group of East Anglia University in the United Kingdom (CRU v4.03) (http://www.cru.uea.ac.uk/cru/data/hrg).

References

Ahmed K, Shahid S, Wang X *et al*., 2019. Spatiotemporal changes in aridity of Pakistan during 1901–2016. *Hy-*

drology and Earth System Sciences, 23(7): 3081–3096.

Allen R G, Pereira L S, Raes D *et al*., 1998. Crop Evapotranspiration: Guidelines for Computing Crop Water Requirements. Roman, Italy: FAO.

Arora V K, 2002. The use of the aridity index to assess climate change effect on annual runoff. *Journal of Hydrology*, 265(1–4): 164–177.

Asadi Zarch MA, Sivakumar B, Sharma A, 2015. Droughts in a warming climate: A global assessment of standardized precipitation index (SPI) and reconnaissance drought index (RDI). *Journal of Hydrology*, 526(2015): 183–195.

Bastos A, Fu Z, Ciais P *et al*., 2020. Impacts of extreme summers on European ecosystems: A comparative analysis of 2003, 2010 and 2018: European extreme summers and the C-cycle. *Philosophical Transactions of the Royal Society B*: *Biological Sciences*, 375(1810): 20190507.

Brando P M, Paolucci L, Ummenhofer C C *et al*., 2019. Droughts, wildfires, and forest carbon cycling: A pantropical synthesis. *Annual Review of Earth and Planetary Sciences*, 47(1): 555–581.

Cao L, Zhou Z, 2019. Variations of the reference evapotranspiration and aridity index over northeast China: Changing properties and possible causes. *Advances in Meteorology*, 2019: 1–13.

Chang P, Saravanan R, Ji L *et al*., 2000. The effect of local sea surface temperatures on atmospheric circulation over the tropical Atlantic sector. *Journal of Climate*, 13(13): 2195–2216.

Cherchi A, Navarra A, 2013. Influence of ENSO and of the Indian Ocean Dipole on the Indian summer monsoon variability. *Climate Dynamics*, 41(1): 81–103.

Cook B I, Smerdon J E, Seager R *et al*., 2014. Global warming and 21st century drying. *Climate Dynamics*, 43(9): 2607–2627.

Dai A, 2012. Increasing drought under global warming in observations and models. *Nature Climate Change*, 3(1): 52–58.

de Oliveira J V, Ferreira D B da S, Sahoo P K *et al*., 2018. Differences in precipitation and evapotranspiration between forested and deforested areas in the Amazon rainforest using remote sensing data. *Environmental Earth Sciences*, 77(6): 1–14.

Donohue R J, Roderick M L, McVicar T R *et al*., 2013. Impact of CO_2 fertilization on maximum foliage cover across the globe's warm, arid environments. *Geophysical Research Letters*, 40(12): 3031–3035.

Feng W, Lu H, Yao T *et al*., 2020. Drought characteristics and its elevation dependence in the Qinghai-Tibet Plateau during the last half-century. *Scientific Reports*, 10(1): 1–11.

Fensholt R, Langanke T, Rasmussen K *et al*., 2012. Greenness in semi-arid areas across the globe 1981–2007: An earth observing satellite based analysis of trends and drivers. *Remote Sensing of Environment*, 121(1): 144–158.

Ficklin D L, Novick K A, 2017. Historic and projected changes in vapor pressure deficit suggest a continental-scale drying of the United States atmosphere. *Journal of Geophysical Research*: *Atmospheres*, 122(4): 2061–2079.

Greve P, Roderick M L, Ukkola A M *et al*., 2019. The aridity index under global warming. *Environmental Research Letters*, 14(12): 124006.

Harris I, Osborn T J, Jones P *et al*., 2020. Version 4 of the CRU TS monthly high-resolution gridded multivariate climate dataset. *Scientific Data*, 7(1): 1–18.

Hoerling M, Eischeid J, Perlwitz J, 2010. Regional precipitation trends: Distinguishing natural variability from anthropogenic forcing. *Journal of Climate*, 23(8): 2131–2145.

Hu Z M, Liang M Q, Knapp A *et al*., 2022. Are regional precipitation-productivity relationships robust to decadal-scale dry period? *Journal of Plant Ecology*, 15(4): 711–720.

Huang J, Ji M, Xie Y *et al*., 2016a. Global semi-arid climate change over last 60 years. *Climate Dynamics*, 46(3):

1131–1150.

Huang J, Li Y, Fu C *et al*., 2017. Dryland climate change: Recent progress and challenges. *Reviews of Geophysics*, 55(3): 719–778.

Huang J, Yu H, Guan X *et al*., 2016b. Accelerated dryland expansion under climate change. *Nature Climate Change*, 6(2): 166–171.

Huang S, Wang L, Wang H *et al*., 2019. Spatio-temporal characteristics of drought structure across China using an integrated drought index. *Agricultural Water Management*, 218(2019): 182–192.

Huo Z, Dai X, Feng S *et al*., 2013. Effect of climate change on reference evapotranspiration and aridity index in arid region of China. *Journal of Hydrology*, 492(1): 24–34.

IPCC, 2021. Climate Change 2021: The Physical Science Basis. Cambridge: Cambridge University Press.

Li L, Yang S, Wang Z *et al*., 2010. Evidence of warming and wetting climate over the Qinghai-Tibet Plateau. *Arctic*, *Antarctic*, *and Alpine Research*, 42(4): 449–457.

Li M, Wu P, Sexton D M H *et al*., 2021. Potential shifts in climate zones under a future global warming scenario using soil moisture classification. *Climate Dynamics*, 56(7): 2071–2092.

Li M, Wu J, Song C *et al*., 2019. Temporal variability of precipitation and biomass of alpine grasslands on the northern Tibetan Plateau. *Remote Sensing*, 11(3): 360.

Li P, Hu Z, Liu Y, 2020. Shift in the trend of browning in southwestern Tibetan Plateau in the past two decades. *Agricultural and Forest Meteorology*, 287(2020): 107950.

Lian X, Piao S, Chen A *et al*., 2021. Multifaceted characteristics of dryland aridity changes in a warming world. *Nature Reviews Earth and Environment*, 2(4): 232–250.

Lickley M, Solomon S, 2018. Drivers, timing and some impacts of global aridity change. *Environmental Research Letters*, 13(10): 10410.

Mu Q, Zhao M, Kimball J S *et al*., 2013. A remotely sensed global terrestrial drought severity index. *Bulletin of the American Meteorological Society*, 94(1): 83–98.

Muñoz-Díaz D, Rodrigo F S, 2005. Influence of the El Niño-Southern Oscillation on the probability of dry and wet seasons in Spain. *Climate Research*, 30(1): 1–12.

Necula A I, Botzan T M, Mariño M A, 1998. Modified de martonne aridity index: Application to the Napa Basin, California. *Physical Geography*, 19(1): 55–70.

Nolan R H, Boer M M, Resco de Dios V *et al*., 2016. Large-scale, dynamic transformations in fuel moisture drive wildfire activity across southeastern Australia. *Geophysical Research Letters*, 43(9): 4229–4238.

Pan N, Wang S, Liu Y *et al*., 2021. Rapid increase of potential evapotranspiration weakens the effect of precipitation on aridity in global drylands. *Journal of Arid Environments*, 186(1): 104414.

Pieper P, Düsterhus A, Baehr J, 2021. Improving seasonal predictions of meteorological drought by conditioning on ENSO states. *Environmental Research Letters*, 16(9): 094027.

Saji N H, Goswami B N, Vinayachandran P N *et al*., 1999. A dipole mode in the tropical Indian Ocean. *Nature*, 401(6751): 360–363.

Saji N H, Yamagata T, 2003. Possible impacts of Indian Ocean Dipole mode events on global climate. *Climate Research*, 25(25): 151–169.

Şarlak N, Mahmood Agha O M A, 2018. Spatial and temporal variations of aridity indices in Iraq. *Theoretical and Applied Climatology*, 133(1): 89–99.

Sheffield J, Wood E F, Roderick M L, 2012. Little change in global drought over the past 60 years. *Nature*, 491(7424): 435–438.

Spinoni J, Naumann G, Vogt J V. 2017. Pan-European seasonal trends and recent changes of drought frequency and severity. *Global and Planetary Change*, 148(1): 113–130.

Strzepek K, Yohe G, Neumann J *et al*., 2010. Characterizing changes in drought risk for the United States from

climate change. *Environmental Research Letters*, 5(4): 044012.

Swann A L S, Hoffman F M, Koven C D *et al*., 2016. Plant responses to increasing CO_2 reduce estimates of climate impacts on drought severity. *Proceedings of the National Academy of Sciences of the United States of America*, 113(36): 10019–10024.

Tsiros I X, Nastos P, Proutsos N D *et al*., 2020. Variability of the aridity index and related drought parameters in Greece using climatological data over the last century (1900–1997). *Atmospheric Research*, 240(1): 104914.

Ullah S, You Q, Sachindra D A *et al*., 2022. Spatiotemporal changes in global aridity in terms of multiple aridity indices: An assessment based on the CRU data. *Atmospheric Research*, 268(1): 105998.

Van Der Schrier G, Barichivich J, Briffa K R *et al*., 2013. A scPDSI-based global data set of dry and wet spells for 1901–2009. *Journal of Geophysical Research*: *Atmospheres*, 118(10): 4025–4048.

Visbeck M H, Hurrell J W, Polvani L *et al*., 2001. The North Atlantic oscillation: Past, present, and future. *Proceedings of the National Academy of Sciences of the United States of America*, 98(23): 12876–12877.

Wu S H, Yin Y H, Zheng D *et al*., 2007. Climatic trends over the Tibetan Plateau during 1971–2000. *Journal of Geographical Sciences*, 17(2): 141–151.

Yang Y, Guan H, Batelaan O *et al*., 2016. Contrasting responses of water use efficiency to drought across global terrestrial ecosystems. *Scientific Reports*, 6(1): 1–8.

Zeng X, Hu Z M, Chen A *et al*., 2022. The global decline in the sensitivity of vegetation productivity to precipitation from 2001–2018. *Global Change Biology*, 28(22): 6823–6833.

Zhao C, Liu B, Piao S *et al*., 2017. Temperature increase reduces global yields of major crops in four independent estimates. *Proceedings of the National Academy of Sciences of the United States of America*, 114(35): 9326–9331.

Zhao W, Hu Z, Guo Q *et al*., 2020. Contributions of climatic factors to interannual variability of the vegetation index in northern China grasslands. *Journal of Climate*, 33(1): 175–183.

Zhou J, Jiang T, Wang Y *et al*., 2020. Spatiotemporal variations of aridity index over the Belt and Road region under the 1.5℃ and 2.0℃ warming scenarios. *Journal of Geographical Sciences*, 30(1): 37–52.

Zhou T J, Chen Z M, Chen X L *et al*., 2021. Interpreting IPCC AR6: Future global climate based on projection under scenarios and on near-term information. *Climate Change Research*, 17(6): 652–663.